Research paper

Static mechanical properties and damage evolution characteristics of selected rocks in diversion tunnel under uniaxial loading

Rongzhou Yang[1], Ying Xu[2], Yonghui Lai[3], Suqian Ni[4], Fengfeng Feng[5]

Abstract: An in-depth understanding of the mechanical properties and damage and fracture mechanism of selected rocks in a diversion tunnel plays an important role in promoting the efficient construction and safety of rock blasting excavation in a diversion tunnel. To study the mechanical properties and damage evolution characteristics of selected rocks in diversion tunnels under uniaxial loading, the uniaxial compression and uniaxial splitting tests of granite and tuff were carried out. In terms of mechanical properties, the evolution characteristics of complete stress-strain curves, instantaneous modulus-strain curves, and input energy density-strain curves were analyzed. In the aspect of damage characteristics, the macroscopic and mesoscopic failure modes were analyzed and the damage fracture mechanism was revealed. Compression-shear failure mainly occurred in granite and tuff under uniaxial compression, showing the characteristics of elastic-brittle fracture failure. Both granite and tuff showed a failure mode of coexistence of "compression-shear failure zone at the loading ends" and "tension-shear failure zone in the middle" under uniaxial splitting. The compression-shear fracture of granite was relatively smooth, and the matrix and mineral particles produced fine particles due to friction in the process of shear slip. The compression-shear fracture of tuff was relatively rough and the characteristics of shear slip were not prominent enough. The fracture failure of granite and tuff was mainly caused by the common fracture of rock matrix and mineral particles. Based on the Lemaitre equivalent strain principle, the pre-peak-post-peak two-stage damage constitutive model established by Weibull statistical distribution theory can accurately describe the static stress-strain relationships of granite and tuff under uniaxial compression.

Keywords: granite/tuff, uniaxial compression, uniaxial splitting, damage evolution, fracture mechanism, damage constitutive model

---

[1]PhD., Eng., School of Civil Engineering and Architecture, Anhui University of Science and Technology, Huainan 232001, China, e-mail: rongzhouy@outlook.com, ORCID: 0000-0002-0126-2446

[2]Prof., PhD., Eng., School of Civil Engineering and Architecture, Anhui University of Science and Technology, Huainan 232001, China, e-mail: yxu@aust.edu.cn, ORCID: 0000-0001-8438-3130

[3]MSc., Eng., Zhejiang Tunnel Engineering Group Co., Ltd., Hangzhou 310000, China, e-mail: laiyonghui121@163.com, ORCID: 0009-0007-9330-7261

[4]MSc., School of Civil Engineering and Architecture, Anhui University of Science and Technology, Huainan 232001, China, e-mail: nisuqian@qq.com, ORCID: 0000-0003-3349-9728

[5]Civil Engineering and Architecture, Anhui University of Science and Technology, Huainan 232001, China, e-mail: 2358834298@qq.com, ORCID: 0009-0007-5828-1115

1. Introduction

Rock blasting fragmentation is the simplest and most basic process of large-scale rock mass engineering (traffic tunnel, diversion tunnel, deep roadway, etc.) [1]. As a material with elastic-brittle characteristics, the tension-compression properties and fracture toughness of rock are the key parameters that affect the safety of engineering structures. The determination of these parameters is very important for the design of underground engineering structures such as mines [2], tunnels, water conservancy, and so on. The deformation, damage, and fracture of rock in the process of loading are the basic reasons for the fragmentation of intact rock [3]. The fracture mechanism of rock blasting is mainly the compression and tension of rock caused by explosion shock waves and detonation gas expansion [4]. Therefore, revealing the mechanical law and damage evolution of rock materials to promote the efficient construction and safety of rock fractures plays an important role, and it is often necessary to carry out rock mechanics tests, especially compression and tensile tests.

Although the rock uniaxial compression test is considered to be a simple rock strength evaluation technique, it leads to complex fracture modes that are difficult to understand in the specimens. Especially, the axial splitting phenomenon was observed in the uniaxial compression test [5]. In terms of the compression test, according to the grain characteristics, Efimov [6] established the failure model of rock samples under uniaxial compression and revealed the failure mechanism of columnar cracks in rock samples along the axial stress direction. Considering that the deterioration of mechanical properties of rock mass has a great influence on the stability of surrounding rock, Mikl-Resch et al. [7] calibrated the yield limit function of rock materials by Brazilian test and uniaxial compression test. Considering that spallation is a form of rock fracture in the uniaxial compression test, it produces an axial splitting plate on the front and side of the cylindrical specimen and then is ejected after buckling, Wang et al. [8] studied the lateral spallation failure mechanism of rock developing parallel to the loading direction. Xiong et al. [9] carried out uniaxial compression and numerical simulation tests on T-type precast fractured rock and studied the effects of fracture and loading direction on uniaxial compressive strength and crack evolution. When evaluating the stability of geotechnical structures, it is necessary to better understand the mechanical behavior of rock under different conditions. Alomari et al [10] studied the effects of physical properties and environmental conditions of sandstone on uniaxial compressive strength and Young's modulus of sandstone and established the prediction equations of compressive strength and Young's modulus of sandstone. Xiong et al. [11] carried out uniaxial compression tests on artificial jointed rock samples with two parallel joints and studied the effects of rock bridge dip angle, joint dip angle, rock bridge length, and joint length on the strength of jointed rock mass. In terms of the splitting tension test, Yang et al. [12] carried out the dynamic and static splitting tensile tests of sandstone using mechanical tests and numerical simulation, and revealed the dynamic and static splitting mechanism of sandstone. According to the distribution

characteristics of the maximum tensile stress around the Griffith fracture and the splitting characteristics of the rock fracture process, Han et al. [13] put forward the axial splitting failure conditions of rock samples, and expounded the splitting fracture mechanism of rock samples. Rabiei et al [14] analyzed the effect of basalt specimen size on crack initiation and crack damage stress limit by the Brazilian tensile test and fracture toughness test. Guan et al. [15] established a theoretical model based on cracking through the Brazilian disk test, and derived the expressions of nominal stress and equivalent crack length, thus providing a comprehensive understanding of the splitting characteristics of rock materials.

The above research results are rich and have played an undeniable role in the development of rock mechanics and engineering technology, promoting efficient construction and safety in rock fracture and fragmentation. However, most of the above studies lack practical engineering background, and the research results are mostly at the theoretical level, without targeted engineering guidance. More importantly, there is a lack of a damage constitutive model that can accurately describe the evolution characteristics of elastic-brittle stress and strain of rock samples to guide engineering practice. This study deeply combined the practical engineering of drilling and blasting rock in the diversion tunnel and conducted uniaxial compression and uniaxial splitting tests on selected rocks (granite and tuff) in the diversion tunnel. It analyzed the typical mechanical properties and damage evolution characteristics of granite and tuff and revealed the macro and meso-damage (meso is a scale level between micro and macro) fracture mechanisms, and a damage constitutive model that can accurately describe the evolution characteristics of elastic-brittle stress and strain of rock samples was established. The results of this study are of great significance for promoting the efficient construction and safety of rock blasting and fragmentation excavation in the diversion tunnel.

2. Preparation method and meso-morphological characteristics of rock samples

2.1. Preparation method of rock samples

The raw materials used in the test were granite and tuff from the drilling and blasting construction section of a diversion tunnel in Zhejiang Province. The in-situ raw rock materials were processed into rock samples (rock samples of two sizes: first of $\Phi = 55$ mm and $h = 110$ mm and second of $\Phi = 55$ mm and $h = 27.5$ mm) through the processes of on-site coring, laboratory cutting, and end face polishing. The specific process of rock sample preparation is shown in Fig. 1. According to the regulations of GB/T 23561-2009 and GB/T 50266-2013, the non-parallelism error between the two ends of the specimen is guaranteed to be less than 0.05 mm. The 120-30AA strain gauges were pasted vertically and horizontally on the surface of rock samples to test the Poisson's ratio of rock samples during the loading test.
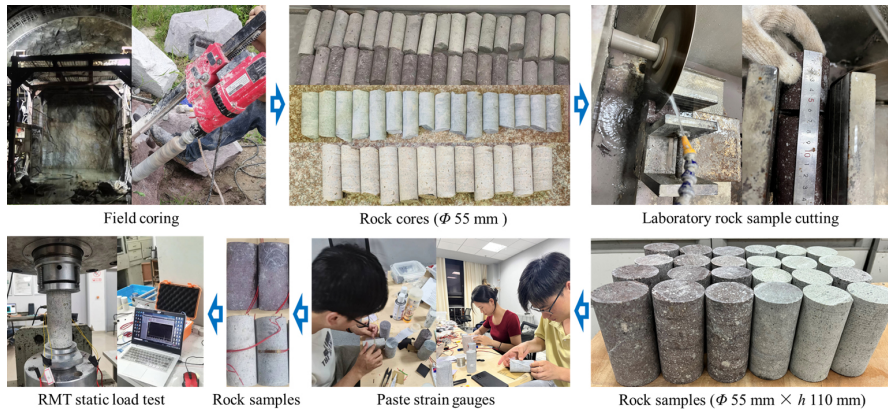
Fig. 1. Preparation process of rock samples

2.2. Meso-morphological characteristics of rock samples

Granite is mainly composed of feldspar, quartz, biotite, hornblende, pyroxene, and other minerals. With the decrease of SiO_2 content and the increase of dark mineral content, its color changes from light gray, reddish brown, and gray-white to dark gray and even black. Granite is a classic plutonic rock formed through extended crystallization of minerals within a magma chamber. In this context, all bonds are characterized by crystallization and are inherently permanent and resistant. Volcanic tuff is a porous pyroclastic rock formed during the sedimentation of materials ejected during a volcanic eruption. It primarily comprises fragments of crushed minerals, volcanic bombs, lapilli, and volcanic ashes that cohesively bond together to create a matrix. Volcanic ashes often contain clay minerals and zeolites as secondary minerals. As a result, tuffs do not possess crystallization bonds like granite but typically exhibit cementation and, occasionally, mechanical bonds.

The meso-morphological characteristics of the cut sections of granite and tuff samples are shown in Fig. 2. As can be seen from Fig. 2, The granite used in the test is mainly composed of brown feldspar, white feldspar, gray-white quartz, and dark biotite or hornblende, while the tuff used in the test is mainly composed of gray-white quartz, white feldspar, a small amount of dark minerals, and accompanied by sediments. In terms of meso-structure, the meso-structural morphologies of granite and tuff are very similar, showing that mineral particles of different sizes and shapes are closely wrapped by rock matrix, and there are some micro-pores and other initial damage. The difference is that in terms of color characteristics, the granite matrix is mainly reddish brown, while the tuff matrix is mainly grayish white. When considering a compacted tuff that has lost its original porosity, and if clay minerals have undergone transformations, it may exhibit some similarities to igneous rocks, such as granite. However, it remains fundamentally distinct from true igneous rocks.

Starting from the meso-structure of materials, meso-damage mechanics distinguishes different meso-damage mechanisms, and understands the damage of materials through the study of the physical and mechanical processes of meso-structural changes. The scale range of meso-
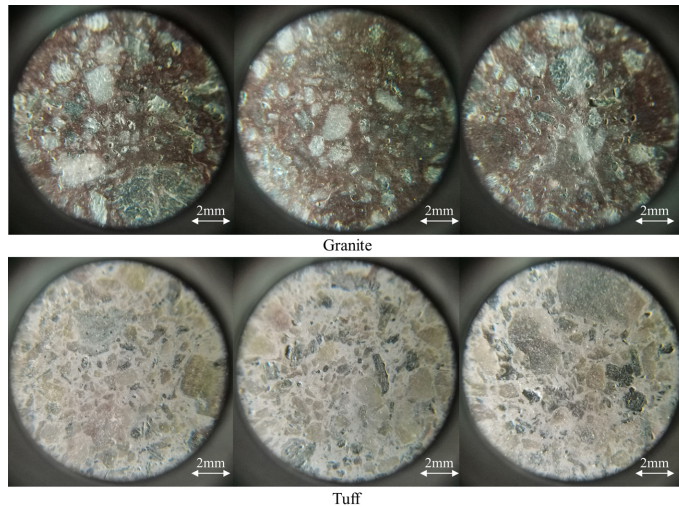
Fig. 2. Meso-morphological characteristics of cutting cross section of rock samples

damage mechanics is between continuum mechanics (macromechanics) and micromechanics. Meso-damage mechanics uses some methods of continuum mechanics and material science to describe the meso-structures such as microvoids, microcracks, and grain boundaries between the two scales. According to meso-damage mechanics [16], under the action of external load, micro-cracks and micro-voids in primary materials will expand and converge, and then form the dynamic evolution process of damage. In other words, the damage of materials and structures begins with the initial damage inside, which determines the mechanical properties of materials and structures [12]. The above meso-structural and morphological characteristics provide a research basis and scientific basis for the following further analysis of mechanical properties.

3. Mechanical properties and damage evolution characteristics

3.1. Loading method and physical and mechanical parameters

By using the RMT-150B electro-hydraulic servo rock mechanics test system (For more information about RMT-150B rock mechanics test system technical parameters, please visit: https://osf.io/w8u95/?view_only=e8aa113f567a44a9b02817e003b2ad49) of the School of Mining Engineering of Anhui University of Science and Technology, the monotonic compression tests of granite and tuff specimens with the size of Φ 55 mm $\times h$ 110 mm and the monotonic splitting tests of granite and tuff specimens with the size of Φ 55 mm $\times h$ 27.5 mm were carried out by means of controlling displacement (the loading rate was 0.005 mm/s). In the uniaxial compression experiments, the longitudinal wave velocity of rock samples was measured by the NM-4B non-metallic ultrasonic analyzer (Fig. 3), and the axial strain and

transverse strain of rock samples were collected by the ST-3C strain testing system to calculate the Poisson's ratio (Fig. 4). The relevant physical and mechanical parameters of granite and tuff are listed in Table 1.
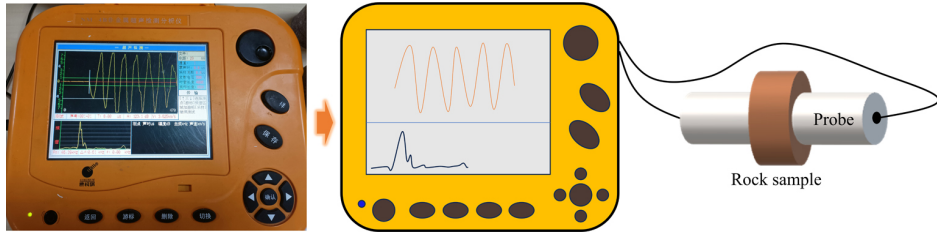

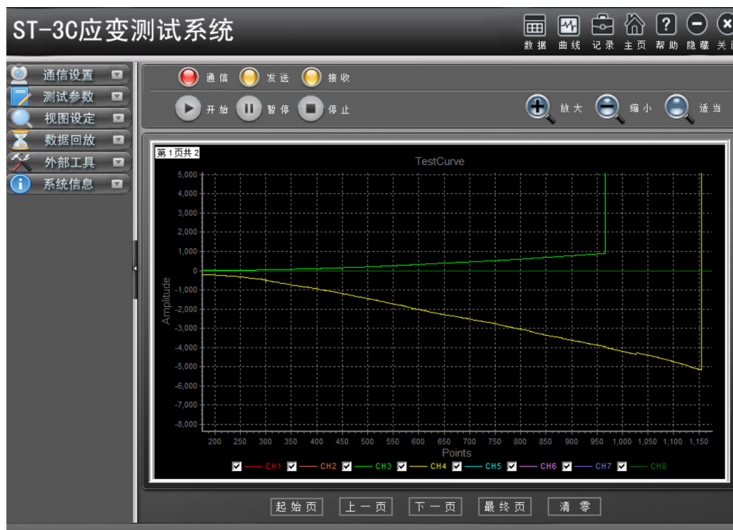Fig. 3. NM-4B non-metallic ultrasonic testing analyzer

Fig. 4. Test interface of ST-3C strain testing system

Table 1. Physical and mechanical parameters of granite and tuff

Rock types	Static compressive strength (MPa)	Static splitting strength (MPa)	Elastic modulus (GPa)	Density (kg/m^3)	Longitudinal wave velocity (m/s)	Poisson's ratio
Granite	134.61	17.72	29.85	2609	4698	0.22
Tuff	113.22	14.98	24.55	2526	4301	0.23

3.2. Evolution characteristics of mechanical properties

(1) Complete stress-strain curves

The complete stress-strain curves of granite and tuff under uniaxial compression are shown in Fig. 5. It can be seen from Fig. 5 that the static compression strength of granite was slightly higher than that of tuff. The evolution characteristics of complete stress-strain curves of granite and tuff under uniaxial compression were very similar. The complete stress-strain curves can be divided into three evolution stages: initial elastic-plastic deformation (OA), pre-peak elastic deformation (AB), and post-peak brittle fracture failure (BC).

1. In the initial elastic-plastic deformation (OA) stage: At this stage, the stress-strain curve of the rock sample showed the characteristic of concave growth and obvious compaction plastic deformation. At the same time, the rock sample also accumulated elastic strain energy in the process of loading. At this stage, the rock sample did not experience any structural damage, and the load level borne by the rock sample at point A was only 35% of the peak load. When the deformation reaches the elastic-plastic deformation limit point A, the stress-strain curve of the rock sample fully enters the stage of linear elastic deformation.

2. In the pre-peak elastic deformation (AB) stage: The stress-strain curve of the rock sample at this stage approximated the growth characteristic of a diagonal straight line, meeting Hooke's law. The rock sample can almost completely convert the input energy of external load into elastic strain energy and store it in the rock sample. At this stage, the rock sample also did not experience significant structural damage, until the load level borne by the rock sample at peak point B approached 100% of the peak load. When the deformation reaches the linear elastic deformation limit point B, the stress-strain curve of the rock sample completely enters the post-peak brittle fracture failure stage.

3. In the post-peak brittle fracture failure (BC) stage: The stress-strain curve of the rock sample at this stage approximated the attenuation characteristic of a vertical straight line, indicating that the elastic deformation energy accumulated by the two stages of elastic plastic deformation (OA) and linear elastic deformation before the peak of the
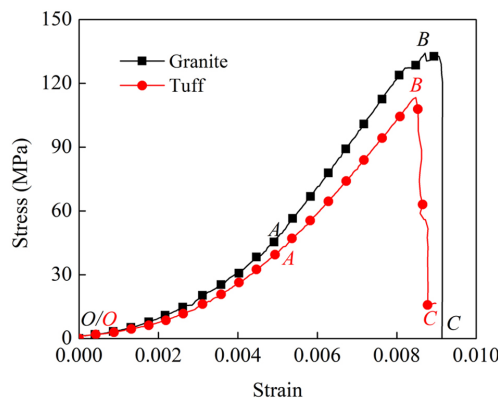

Fig. 5. Complete stress-strain curves of granite and tuff under uniaxial compression

rock sample was instantly released at point B of the linear elastic deformation limit. The elastic strain energy mainly converted the fracture failure energy and fragment ejection energy of the rock sample, and the rock sample underwent complete structural damage. Both granite and tuff exhibited significant elastic-brittle characteristics as a whole.

(2) Instantaneous modulus-strain curves

The instantaneous modulus is the modulus of a rock sample at any time in the process of uniaxial compression, which can be obtained by the derivative of the stress-strain curve. The instantaneous modulus-strain curves of granite and tuff under uniaxial compression are shown in Fig. 6. From Fig. 6, it can be seen that from the overall evolution characteristics of the instantaneous modulus-strain curves, the static instantaneous modulus of granite was slightly greater than that of tuff. The evolution characteristics of the instantaneous modulus-strain curves of granite and tuff under uniaxial compression were very similar. Combined with the evolution characteristics of the complete stress-strain curves, the instantaneous modulus-strain curve can be divided into two evolution stages: linear fluctuation growth (OA) and horizontal fluctuation stability (AB).

1. In the linear fluctuation growth (OA) stage: It can be seen that the instantaneous modulus of the rock sample at this stage was approximately characterized by a linear fluctuation growth evolution, indicating that as the increase of strain, the compression plastic deformation of the rock sample gradually shifted towards elastic deformation. It is worth noting that when the strain reaches 0.003, the fluctuation amplitude of the instantaneous modulus significantly increases, indicating that during the initial compaction plastic deformation stage, the instantaneous modulus appears relatively stable due to easy deformation. However, when the compaction plastic deformation of the rock sample gradually transitions to elastic deformation, the instantaneous modulus will appear relatively unstable due to relatively difficult deformation.

2. In the horizontal fluctuation stability (AB) stage: It can be seen that the instantaneous modulus of the rock sample at this stage was approximately characterized by a stable evolution of horizontal fluctuations, indicating that the rock sample basically enters the
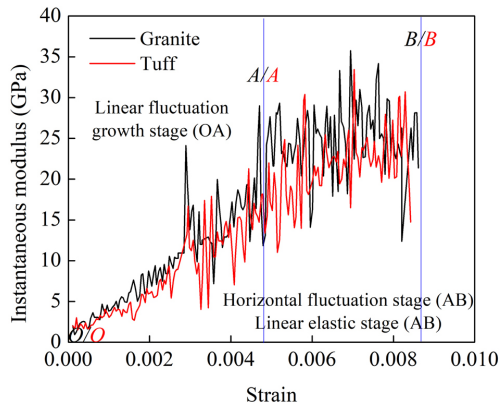

Fig. 6. Instantaneous modulus-strain curves of granite and tuff under uniaxial compression

linear elastic deformation stage at the elastic-plastic deformation limit point A. At this stage, the instantaneous modulus of the rock sample continued to exhibit significant fluctuations, exhibiting obvious elastic deformation characteristics. It is worth noting that when approaching the linear elastic deformation limit point B, the instantaneous modulus shows a slight decrease trend, indicating that the rock sample has undergone slight structural damage towards the peak point B, indicating that the rock sample will reach the bearing limit and energy storage limit at point B.

(3) Input energy density-strain curves

The input energy density-strain curves of granite and tuff under uniaxial compression are shown in Fig. 7. From Fig. 7, it can be seen that from the overall evolution characteristics of the input energy density-strain curves, the energy storage limit of granite was slightly greater than that of tuff. The evolution characteristics of the input energy density-strain curves of granite and tuff under uniaxial compression were very similar. Combined with the evolution characteristics of the complete stress-strain curves, the input energy density-strain curve can be divided into three evolutionary stages: initial slow growth (OA), pre-peak rapid growth (AB), and post-peak continuous growth (BC).

1. In the initial slow growth (OA) stage: The input energy increases slowly due to the initial compaction plastic deformation, and the energy growth rate increases due to the accumulation of elastic strain energy.

2. In the pre-peak rapid growth (AB) stage: The input energy gradually reaches the maximum with the increase of strain, which means that in this stage, the input energy is mainly transformed into elastic strain energy and accumulated in the rock sample.

3. In the post-peak continuous growth (BC) stage: In the process of post-peak fracture failure, rock samples still require the continuous input of external energy, but the energy driving the fracture failure of rock samples mainly comes from the large amount of elastic strain energy accumulated in the pre-peak.
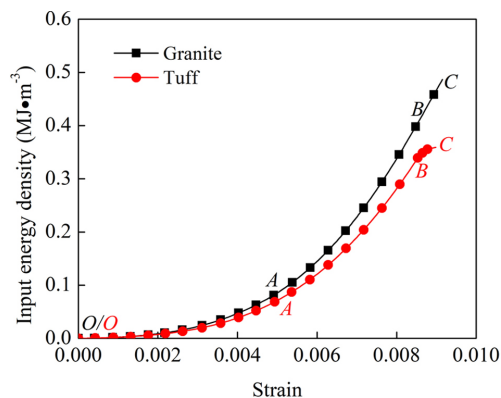

Fig. 7. Input energy density-strain curves of granite and tuff under uniaxial compression

From the analysis of the relationship between energy transformation and deformation characteristics, it is known that in the process of loading, the irreversible deformation of rock samples due to compaction energy dissipation or damage energy dissipation is plastic

deformation, and the dissipated energy of rock samples in this process is plastic strain energy. The reversible deformation of rock samples due to energy accumulation is elastic deformation, and the accumulated energy of rock samples in this process is elastic strain energy.

3.3. Failure modes and damage fracture mechanism

(1) Macro-failure modes and damage fracture mechanism

The macro-failure modes of granite and tuff under uniaxial compression and splitting are shown in Figs. 8 and 9. It can be seen from Fig. 8 that the failure mode of granite under uniaxial compression was mainly compression-shear and split-tension failure, accompanied by strong rockburst phenomenon, fragment ejection phenomenon was obvious, showing significant elastic-brittle fracture failure characteristics. The failure mode of tuff under uniaxial compression was mainly the compression-shear and spalling failure, the failure process was relatively stable, and the fragment ejection phenomenon was not obvious, but it also showed obvious elastic-brittle fracture failure characteristics.

It can be seen from Fig. 9 that the macro-failure modes of granite and tuff under uniaxial splitting were similar, showing the coexistence of the "compression-shear failure zone at the loading ends" and "tension-shear failure zone in the middle". In the loading direction, the characteristics of the split rock blocks in the middle of the rock samples were more prominent due to the tension-shear action in the middle.

Granite   Tuff
Fig. 8. Macro-damage failure states of granite and tuff under uniaxial compression

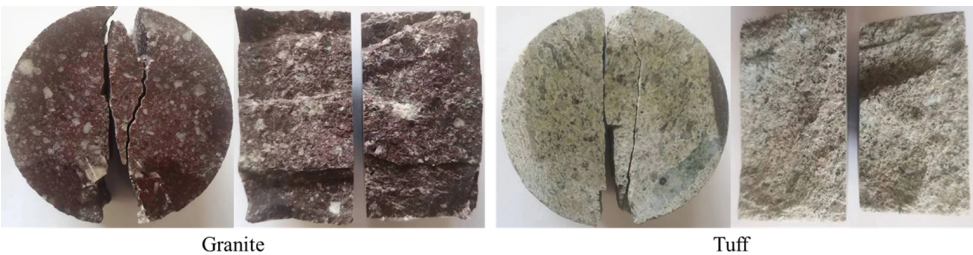Granite   Tuff
Fig. 9. Macro-damage failure states of granite and tuff under uniaxial splitting

(2) Meso-failure modes and damage and fracture mechanism

The meso-damage states of the compression-shear fracture of granite and tuff under uniaxial compression are shown in Fig. 10. As can be seen from Fig. 10, the compression-shear fracture of granite was relatively smooth, and there was an obvious layer of rock fine particles on the fracture surfaces, which was caused by friction between granite matrix and mineral particles in the process of shear slip. The fine rock particles distributed on the fracture surfaces cover up the distribution characteristics of the reddish brown matrix and mineral particles of granite to some extent. However, the compression-shear fracture of tuff was relatively rough, meso-structural morphology was clearly visible, and the shear slip characteristic was not prominent, the main reason is that the rock fine particles distributed on the tuff fracture surfaces are mainly formed by the friction of the gray-white matrix of tuff in the process of shear slip, and the rock fine particles are mainly single gray-white, which is different from granite.

The meso-damage states of split-tension fracture of granite and tuff under uniaxial compression are shown in Fig. 11. As can be seen from Fig. 11, from the fracture morphology, compared with the compression-shear fracture, the split-tension fracture of granite and tuff was very rough, and the color of the rock matrix and mineral distribution characteristics were clearly visible on the fracture surfaces, and there were many micro-cracks and micro-pores. The fracture failure of granite and tuff was mainly caused by the common fracture of rock matrix and mineral particles. According to the principle of minimum energy, under the action of external load, the initial defects such as primary micro-cracks and micro-pores in rock samples become the starting point of rock sample damage due to stress concentration; the reason is that the energy consumption of fracture damage at the initial defects is the least, it is easier to produce damage, and then under the continuous action of external load, the initial defects expand and converge, thus forming the dynamic evolution process of damage.
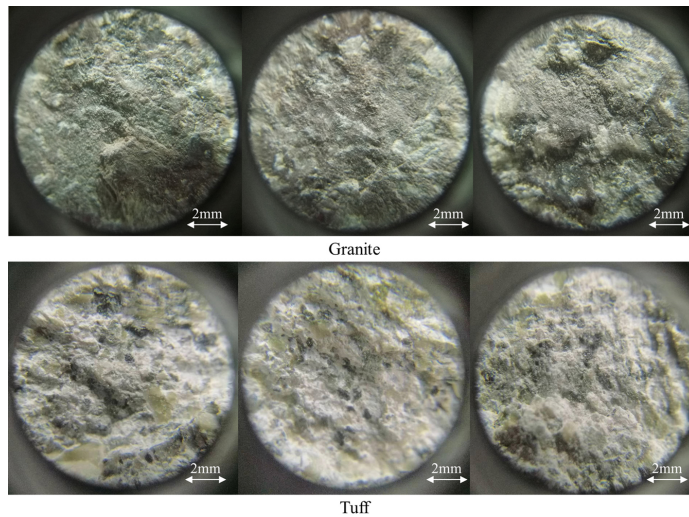

Granite

Tuff

Fig. 10. Meso-damage failure states of compression-shear fracture of granite and tuff under uniaxial compression
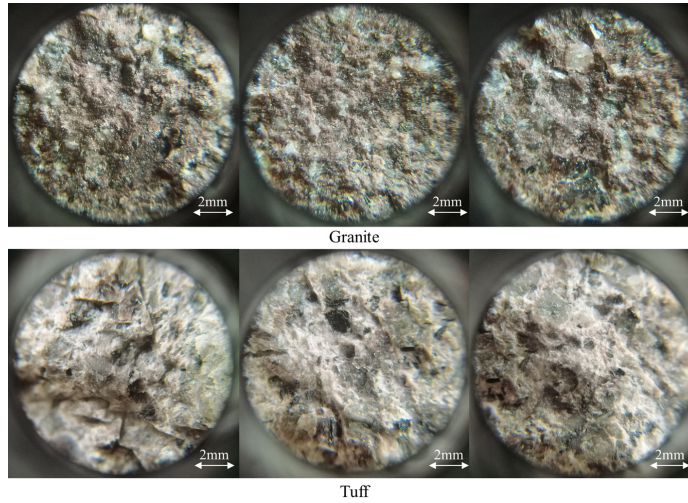
Fig. 11. Meso-damage failure states of split-tension fracture of granite and tuff under uniaxial splitting

4. Pre-peak-post-peak two-stage damage constitutive model for static uniaxial compression

4.1. Establishment of damage constitutive model

The so-called damage mechanics refers to the development law and deterioration mechanism of material damage with the change of deformation or time in various environments [17]. According to Lemaitre's strain equivalence hypothesis [18, 19], the effect of damage on strain behavior is reflected by effective stress, that is, the strain generated by nominal stress on the damaged material is equal to the strain generated by effective stress on the non-damaged material. This hypothesis can be represented by Eq. (4.1) under one-dimensional stress state [18, 19]:

$$\sigma = E(1 - D) \tag{4.1}$$

where: σ – stress, E – elastic modulus, ε – strain, D – damage variable.

Considering the damage and failure of rock samples as a continuous development process, it can be assumed that [20]: (1) The rock sample is macroscopically considered isotropic, and the damage and failure exhibit isotropic equivalent development; (2) Consider the rock sample as a macroscopic combination composed of internal countless micro elements, which contain many randomly distributed micro cracks and small defects.

In essence, the energy dissipated by material damage is a comprehensive reflection of the changes of strength and deformation in the process of material damage [21]. Therefore, from the point of view of the internal defects of rock samples, if any micro-element is taken, its

damage dissipation energy must obey a specific statistical law. It can be selected that the damage dissipation energy of the micro-element obeys the Weibull distribution Eq. (4.2) [22–24]:

$$(4.2) \qquad f(U) = \frac{b}{a} \left(\frac{U}{a} \right)^{b-1} \exp \left[- \left(\frac{U}{a} \right)^b \right]$$

where: U – the distribution variable of micro-element damage dissipation energy, a and b – the parameters related to damage.

The damage variable D in Eq. (4.1) is a measure that characterizes the degree of material damage, and the D is related to the number of defects contained in each micro-element, which directly affects the damage dissipation energy U of the micro-element. The statistical law that the D and the U follow is Eq. (4.3):

$$(4.3) \qquad \frac{dD}{dU} = f(U)$$

Substitute Eq. (4.3) into Eq. (4.2), and integrate to obtain [22–24]:

$$(4.4) \qquad D = \int_0^\varepsilon f(U) dU = 1 - \exp \left[- \left(\frac{\varepsilon}{a} \right)^b \right]$$

Eq. (4.4) is a damage evolution equation based on the assumption that the distribution function of damage dissipation energy of micro-elements in rock materials satisfies Weibull distribution. Based on Eq. (4.4), Eq. (4.1) can be rewritten as Eq. (4.5):

$$(4.5) \qquad \sigma = E\varepsilon \exp \left[- \left(\frac{\varepsilon}{a} \right)^b \right]$$

Rock materials are not ideal brittle materials, as they exhibit certain initial compaction behavior before the peak due to their plastic characteristics, and exhibit elastic-brittle fracture behavior after the peak. To effectively and accurately reproduce the compaction and fracture behavior of such materials, it is necessary to further revise the constitutive Eq. (4.5) initially established using Weibull statistical distribution theory, especially the damage constitutive model that can reflect the compaction effect in the pre-peak stage of the stress-strain curves.

Combined with the plastic characteristics of the damage constitutive model of post-peak stress-strain curves of concrete materials, the following results can be obtained [25]:

$$(4.6) \qquad \sigma = c \exp \left\{ -\frac{1}{2} \left[\frac{\ln \left(\frac{\varepsilon}{l} \right)}{u} \right]^2 \right\}$$

where: c, u, and l – shape parameters.

According to the boundary geometric conditions: (1) $\varepsilon = \varepsilon_p$ (peak strain) and $\sigma = \sigma_p$ (peak stress); (2) $\varepsilon = \varepsilon_p$ and $d\sigma/d\varepsilon = 0$. The derivative of Eq. (4.6) can be obtained:

$$(4.7) \qquad \frac{d\sigma}{d\varepsilon} = -c \frac{\ln \left(\frac{\varepsilon}{l} \right)}{u^2 \varepsilon} \exp \left\{ -\frac{1}{2} \left[\frac{\ln \left(\frac{\varepsilon}{l} \right)}{u} \right]^2 \right\}$$

Substituting the boundary geometric condition (2) into Eq. (4.7) yields:

$$(4.8) \qquad\qquad l = \varepsilon_p$$

Substituting boundary geometric conditions (1) and Eq. (4.8) into Eq. (4.6) yields:

$$(4.9) \qquad\qquad c = \sigma_p$$

The damage constitutive model of post-peak stress-strain curves of concrete materials can be obtained [25]:

$$(4.10) \qquad\qquad \sigma = \sigma_p \exp\left\{ -\frac{1}{2}\left[\frac{\ln\left(\frac{\varepsilon}{\varepsilon_p}\right)}{u} \right]^2 \right\}$$

Considering the significant initial compaction stage before the peak in the stress-strain curve of rock samples under uniaxial compression, unfortunately, many damage constitutive equations cannot describe this stage well or directly ignore the pre-peak compaction stage. But at the same time, it was found that the initial compaction stage before the peak and the later softening stage after the peak of the concrete material roughly exhibit symmetrical evolutionary characteristics geometrically. Therefore, by combining the geometric symmetry similarity before and after the peak, we can further better characterize the pre-peak stress-strain curves and damage evolution characteristics of rock materials under uniaxial compression.

By combining calculations, the pre-peak damage constitutive model of the rock samples under uniaxial compression can be further obtained [23]:

$$(4.11) \qquad \sigma = \frac{1}{2}E\varepsilon \exp\left[-\left(\frac{\varepsilon}{a}\right)^b \right] + \frac{1}{2}\sigma_p \exp\left\{ -\frac{1}{2}\left[\frac{\ln\left(\frac{\varepsilon}{\varepsilon_p}\right)}{u} \right]^2 \right\}$$

Combined with the evolution characteristics of full stress-strain curves of rock samples under uniaxial compression, the post-peak stress-strain curves show significant elastic-brittle characteristics. Therefore, the post-peak damage constitutive model of rock samples under uniaxial compression can be further obtained:

$$(4.12) \qquad\qquad \sigma = 0$$

To sum up, a pre-peak-post-peak two-stage damage constitutive model which can describe the evolution characteristics of full stress-strain curves of rock samples under uniaxial compression can be obtained:

$$(4.13) \qquad \sigma = \begin{cases} \dfrac{1}{2}E\varepsilon \exp\left[-\left(\dfrac{\varepsilon}{a}\right)^b \right] + \dfrac{1}{2}\sigma_p \exp\left\{ -\dfrac{1}{2}\left[\dfrac{\ln\left(\dfrac{\varepsilon}{\varepsilon_p}\right)}{u} \right]^2 \right\} & (\varepsilon \le \varepsilon_p) \\[20pt] 0 & (\varepsilon > \varepsilon_p) \end{cases}$$

4.2. Comparative analysis of theoretical curves and experimental curves

The stress-strain curves calculated by the damage constitutive model were compared with the experimental data (Figs. 12 and 13). It can be seen from Figs. 12 and 13 that the stress-strain curves calculated by the model were basically consistent with the stress-strain curves obtained by the tests, and the correlation coefficient (*R-square*) was more than 0.99, which fully reflected the initial plastic compaction deformation and post-peak elastic brittle failure characteristics of the stress-strain curves. Therefore, the pre-peak-post-peak two-stage damage constitutive model established in this work can well describe the full stress-strain relationship of granite and tuff under uniaxial compression.
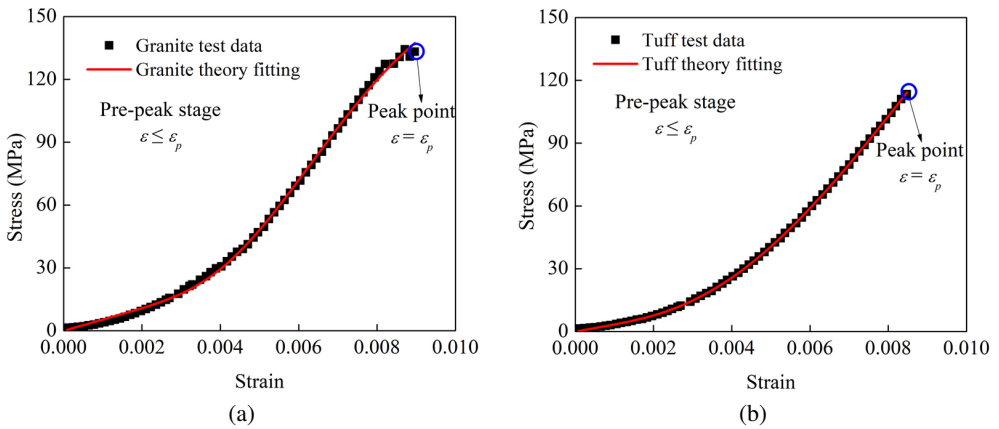
Fig. 12. Pre-peak damage constitutive model fitting curves of granite and tuff under uniaxial compression; (a) Granite (b) Tuff
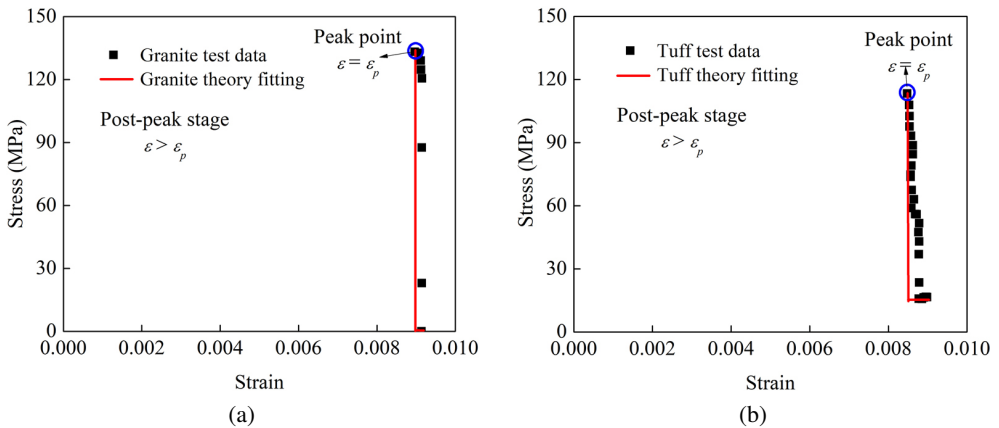
Fig. 13. Post-peak damage constitutive model fitting curves of granite and tuff under uniaxial compression; (a) Granite (b) Tuff

5. Conclusions

1. The complete stress-strain curves of granite and tuff showed three evolution stages: initial elastic-plastic deformation, pre-peak elastic deformation, and post-peak brittle fracture failure. The instantaneous modulus-strain curves of granite and tuff showed two evolution stages: linear fluctuation growth and horizontal fluctuation stability. The input energy density-strain curves of granite and tuff showed three evolution stages: initial slow growth, pre-peak rapid growth, and post-peak continuous growth.

2. Compression-shear and split-tension failure mainly occurred in granite under uniaxial compression, accompanied by strong rockburst phenomenon, fragment ejection phenomenon was obvious, showing significant elastic-brittle fracture failure characteristics. Tuff mainly occurred compression-shear and spalling failure under uniaxial compression, the failure process was relatively stable, and the fragment ejection phenomenon was not obvious, but it also showed obvious elastic-brittle fracture failure characteristics. Both granite and tuff showed a failure mode of coexistence of "compression-shear failure zone at the loading ends" and "tension-shear failure zone in the middle" under uniaxial splitting.

3. The compression-shear fracture surfaces of granite were relatively smooth, and the matrix and mineral particles produced fine particles due to friction in the process of shear slip. However, the compression-shear fracture surfaces of tuff were relatively rough, meso-structural morphology was clearly visible, and the shear slip characteristic was not prominent enough. The split-tension fracture surfaces of granite and tuff were rough, the color of the rock matrix and mineral distribution characteristics were clearly visible on the section, and there were many micro-fractures and micro-pores. The fracture failure of granite and tuff was mainly caused by the common fracture of rock matrix and mineral particles.

4. Based on the Lemaitre equivalent strain principle, the pre-peak-post-peak two-stage damage constitutive model established by Weibull statistical distribution theory can accurately describe the static stress-strain relationships of granite and tuff under uniaxial compression, which effectively reflected the pre-peak compaction effect of rock samples.

Acknowledgements

References

[1] Z. Li, Y. Hu, G. Wang, M. Zhou, W. Hu, X. Zhang, and W. Gao, "Study on cyclic blasting failure characteristics and cumulative damage evolution law of tunnel rock mass under initial in-situ stress", *Engineering Failure Analysis*, vol. 150, 2023, doi: 10.1016/j.engfailanal.2023.107310.

[2] W. Jing, Y. Gao, R. Jin, and L. Jing, "Deformation failure analysis and identification method of zoning type of actual tunnel surrounding rock", *Archives of Civil Engineering*, vol. 69, no. 4, pp. 549–571, 2023, doi: 10.24425/ace.2023.147676.

[3] L. Guo, X. Wang, Z. Xu, P. Li, and X. Liu, "Research on the Concept of Rock Energy Body and Rock Fragmentation Index", *Metal Mine*, 2023 [Online]. Available: http://kns.cnki.net/kcms/detail/34.1055.TD. 20230320.1032.006.html.

[4] R. Yang, Y. Xu, J. Liu, J. Ding, and H. Xie, "Dynamic damage characteristics of two-dimensional flat plate of rigid-flexible coupling surrounding rock supporting structure under blast loading", *Journal of Central South University(Science and Technology)*, vol. 54, no. 6, pp. 2513–2528, 2023, doi: 10.11817/j.issn.1672-7207.2023.06.036.

[5] A. Fakhimi and Behzad Hemami, "Axial splitting of rocks under uniaxial compression", *International Journal of Rock Mechanics and Mining Sciences*, vol. 79, pp. 124–134, 2015, doi: 10.1016/j.ijrmms.2015.08.013.

[6] V.P. Efimov, "Features of uniaxial compression failure of brittle rock samples with regard to grain characteristics", *Journal of Mining Science*, vol. 54, pp. 194–201, 2018, doi: 10.1134/S1062739118023545.

[7] M.J. Mikl-Resch, T. Antretter, M. Gimpel, H. Kargl, G. Pittino, R. Tichy, W. Ecker, and R. Galler, "Numerical calibration of a yield limit function for rock materials by means of the Brazilian test and the uniaxial compression test", *International Journal of Rock Mechanics and Mining Sciences*, vol. 74, pp. 24–29, 2015, doi: 10.1016/j.ijrmms.2014.12.001.

[8] H. Wang, A. Dyskin, E. Pasternak, and P. Dight, "Possible mechanism of spallation in rock samples under uniaxial compression", *Engineering Fracture Mechanics*, vol. 269, 2022, doi: 10.1016/j.engfracmech.2022.108577.

[9] L. Xiong, H. Chen, Z. Xu, and D. Hu, "Uniaxial compression test and numerical simulation of rock-like specimen with T-Shaped cracks", *Archives of Civil Engineering*, vol. 69, no. 2, pp. 227–244, 2023, doi: 10.24425/ace.2023.145265.

[10] E.M. Alomari, K.W. Ng, L. Khatri, and S.S. Wulff, "Effect of physical properties on mechanical behaviors of sandstone under uniaxial and triaxial compressions", *Materials*, vol. 16, no. 13, 2023, doi: 10.3390/ma16134867.

[11] L.X. Xiong, H.Y. Yuan, Y. Zhang, K.F. Zhang, and J. B. Li, "Experimental and numerical study of the uniaxial compressive stress-strain relationship of a rock mass with two parallel joints", *Archives of Civil Engineering*, vol. 65, no. 2, pp. 67–80, 2019, doi: 10.2478/ace-2019-0019.

[12] R. Yang, Y. Xu, J. Liu, J. Ding, and H. Xie, "Comparative analysis of dynamic mechanics and failure characteristics of sandstone and quasi-sandstone material", *Materials Reports*, vol. 37, no. 23, 2023, doi: 10.11896/cldb.22030265.

[13] L. Han, Y. He, and H. Zhang, "Study of rock splitting failure based on griffith strength theory", *International Journal of Rock Mechanics and Mining Sciences*, vol. 83, pp. 116–121, 2016, doi: 10.1016/j.ijrmms.2015.12.011.

[14] M. Rabiei, P. Samea, A. Shadi, and S.A. Ghoreishi-Madiseh, "A discrete element analysis for general failure behavior of basalt", *International Journal of Rock Mechanics and Mining Sciences*, vol, 167, 2023, doi: 10.1016/j.ijrmms.2023.105394.

[15] J. Guan, S. Wang, L. Li, C. Xie, M. Khan, and L. Niu, "Design of rock material parameters by cracked straight through Brazilian disc", *Construction and Building Materials*, vol. 402, 2023, doi: 10.1016/j.conbuildmat.2023.133049.

[16] Y. Toi and J. Che, "Computational damage mechanics models for brittle microcracking solids based on mesoscopic simulation", *Engineering Fracture Mechanics*, vol. 48, no. 4, pp. 483–498, 1994, doi: 10.1016/0013-7944(94)90203-8.

[17] N. Nie, "Prediction of concrete life under coupled dry and wet-sulfate erosion based on damage evolution equation", *Archives of Civil Engineering*, vol. 69, no. 4, pp. 679–692, 2023, doi: 10.24425/ace.2023.147683.

[18] J. Lemaitre, "How to use damage mechanics", *Nuclear Engineering and Design*, vol. 80, no. 2, pp. 233–245, 1984, doi: 10.1016/0029-5493(84)90169-9.

[19] J. Lemaitre, "Local approach of fracture", *Engineering Fracture Mechanics*, vol. 25, no. 5-6, pp. 523–537, 1986, doi: 10.1016/0013-7944(86)90021-4.

[20] Z. Wan, K. Ma, G. Long, and Y. Xie, "A fatigue damage constitutive model of SCC based on Weibull distribution and residual strain", *Materials Reports*, vol. 33, no. 4, pp. 634–638, 2019, doi: 10.11896/cldb.201904013.

[21] R. Yang, Y. Xu, P. Chen, L. Cheng, J. Ding, and H. Fu, "Experimental study on SHPB cyclic impact of rubber-cement composite with different confine modes", *Archives of Civil Engineering*, vol. 69, no. 2, pp. 517–534, 2023, doi: 10.24425/ace.2023.145282.

[22] W. Weibull, "A statistical distribution function of wide applicability", *Journal Applied Mechanics*, vol. 18, no. 3, pp. 293–297, 1951, doi: 10.1115/1.4010337.

[23] R. Yang, Y. Xu, P. Chen, and J. Gong, "Static compressive properties and damage constitutive model of rubber cement mortar with dry- and wet-curing conditions", *Journal of Central South University*, vol. 28, no. 7, pp. 2158–2178, 2021, doi: 10.1007/s11771-021-4763-1.

[24] S.M.A. Aljeddani and M.A. Mohammed, "A novel approach to Weibull distribution for the assessment of wind energy speed", *Alexandria Engineering Journal*, vol. 78, pp. 56–64, 2023, doi: 10.1016/j.aej.2023.07.027.

[25] Q. Wang, "Study on dynamic damage characteristics of steel fiber reinforced concrete", Yichang: Three Gorges University, 2009, doi: 10.7666/d.d066359.